

Investigating enhanced Aqua MODIS aerosol optical depth retrievals over the mid-to-high latitude Southern Oceans through intercomparison with co-located CALIOP, MAN, and AERONET data sets

Travis D. Toth,¹ Jianglong Zhang,¹ James R. Campbell,² Jeffrey S. Reid,² Yingxi Shi,¹ Randall S. Johnson,¹ Alexander Smirnov,³ Mark A. Vaughan,⁴ and David M. Winker⁴

Received 16 October 2012; revised 24 January 2013; accepted 3 March 2013; published 29 May 2013.

[1] A band of enhanced aerosol optical depth (AOD) over the mid-to-high latitude Southern Oceans exists in some passive satellite-based aerosol data sets, including Moderate Resolution Imaging Spectroradiometer (MODIS) products. Past studies suggest several potential causes contributing to this phenomenon, including signal uncertainty, retrieval bias, and cloud contamination. In this paper, quality-assured Aqua MODIS aerosol products in this zonal band are investigated to assess cloud contamination as a cause. Spatially and temporally collocated cloud and aerosol products produced by the Cloud-Aerosol Lidar with Orthogonal Polarization (CALIOP) project relative to Aqua MODIS AOD in this region are considered. Maritime Aerosol Network (MAN) and Aerosol Robotic Network (AERONET) AOD data are also collocated with Aqua MODIS retrievals for surface context. The results of this study indicate that the high Aqua MODIS AOD are not seen in the CALIOP aerosol products, cannot be screened using active profiling of collocated observations for cloud presence, and are not detected by ground-based observations such as MAN and AERONET. Enhanced AOD values are attributable primarily to stratocumulus and low broken cumulus cloud contamination, as identified with CALIOP products. But these clouds explain only about 30–40% of the total anomaly. Cirrus cloud contamination is also a factor. However, in contrast to the rest of the globe, they contribute less overall, relative to low-level liquid water clouds, which are considered likely the result of misidentification of relatively warm cloud tops compared with surrounding open seas.

Citation: Toth, T. D., J. Zhang, J. R. Campbell, J. S. Reid, Y. Shi, R. S. Johnson, A. Smirnov, M. A. Vaughan, and D. M. Winker (2013), Investigating enhanced Aqua MODIS aerosol optical depth retrievals over the mid-to-high latitude Southern Oceans through intercomparison with co-located CALIOP, MAN, and AERONET data sets, *J. Geophys. Res. Atmos.*, 118, 4700–4714, doi:10.1002/jgrd.50311.

1. Introduction

[2] Remotely sensed measurements from satellites provide a unique view of aerosol distributions across the globe [e.g., Wielicki *et al.*, 1995; Jaegle *et al.*, 2011]. However, current satellite-based retrievals of aerosol optical properties are subject to signal uncertainty, algorithm bias, and cloud

contamination [e.g., Kaufman *et al.*, 2005; Zhang and Reid, 2006]. If not properly filtered and/or accommodated for a thorough quality assurance (QA) screening, systematic biases in these data sets can significantly compromise resolution and closure of aerosol radiative and physical processes for advanced climate assessment [e.g., Zhang *et al.*, 2008; Zhang and Reid, 2009].

[3] One unique example of potential signal bias has been found in aerosol optical depth (AOD) data sets collected by some passive satellite instruments over the mid-to-high latitude Southern Oceans (defined from 45°S to 65°S), where an intermittent band of relatively high AOD is found [e.g., Zhang and Reid, 2006; Shi *et al.*, 2011]. Initial assessments suggest that this was due to the production of sea salt particles by the typically near-surface high winds occurring along this zonal band [e.g., Lehahn *et al.*, 2010; Madry *et al.*, 2011]. However, the first passive multisensor and multi-algorithm intercomparisons showed widely varying results here, thus suggesting another predominant physical

¹Department of Atmospheric Sciences, University of North Dakota, Grand Forks, North Dakota, USA.

²Aerosol and Radiation Sciences Section, Marine Meteorology Division, Naval Research Laboratory, Monterey, California, USA.

³Sigma Space Corporation, Greenbelt, Maryland, USA.

⁴NASA Langley Research Center, Hampton, Virginia, USA.

Corresponding author: J. Zhang, Department of Atmospheric Sciences, 4149 University Avenue Stop 9006, University of North Dakota, Grand Forks, ND 58202, USA. (jzhang@atmos.und.edu)

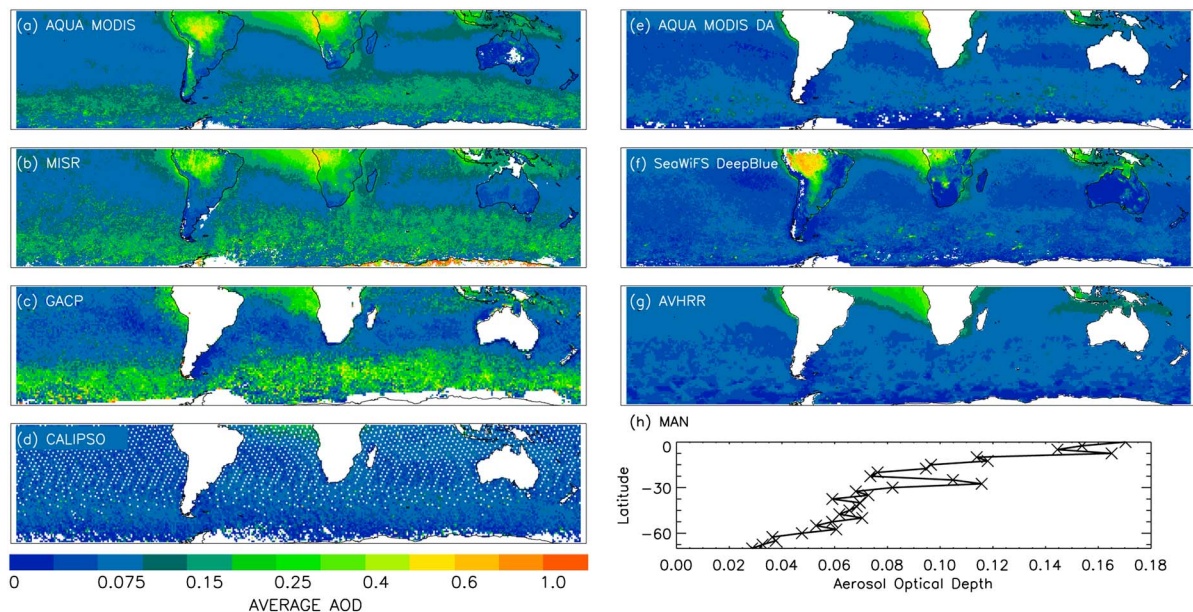


Figure 1. From 2005, annual mean global AOD composites derived from (a) Aqua MODIS Collection 5.1 over-ocean “marginal” and over-land “good” data sets, (b) MISR Version 22 data sets, using “successful” retrieval flag, (c) Global Aerosol Climatology Project data sets. 2007–2009 annual mean global AOD composite derived from (d) CALIOP. From 2005, annual mean global AOD composites derived from (e) Aqua MODIS Collection 5 Data Assimilation Quality data sets, (f) SeaWiFS DeepBlue Level 3 Version 3, (g) the AVHRR AERO100 product, (h) Zonal mean AOD from MAN (2004–2011). Figures 1a, 1b, and 1f are displayed at $0.5^\circ \times 0.5^\circ$ resolution, while Figures 1c–1e and 1g are depicted at $1.0^\circ \times 1.0^\circ$ resolution. See the text for reference and further information relating to the data sets used here.

mechanism. For example, *Myhre et al.* [2004, 2005] describe such variability for Global Aerosol Climatology Project (GACP) and Advanced Very High Resolution Radiometer (AVHRR) products, respectively. Similarly, they show Moderate Resolution Imaging Spectroradiometer (MODIS) and Sea-viewing Wide Field-Of View Sensor (SeaWiFS) products exhibiting significant differences as well. Even after multiple product line updates, the divergence between retrievals reported by *Myhre et al.* [2004, 2005] still exists today.

[4] The scenario for Enhanced Southern Oceans AOD (hereafter referred to as ESOA) [*Gao et al.*, 2002; *Zhang et al.*, 2005; *Zhang and Reid*, 2006] is depicted in Figure 1. From 2005, $0.5^\circ \times 0.5^\circ$ averaged AOD from 70°S to 0°S is shown from Collection 5.1 MODIS retrievals based on measurements collected aboard the Aqua satellite platform (hereafter referred to simply as MODIS; Figure 1a) [*Remer et al.*, 2005], for over-ocean “marginal” and over-land “good” QA flags, Multi-angle Imaging Spectroradiometer (MISR) Version 22 retrievals for “successful” QA flags (Figure 1b) [*Diner et al.*, 1998], and SeaWiFS DeepBlue Level 3 Version 3 (Figure 1f) [*Sayer et al.*, 2012]. For the same year, 1.0° by 1.0° averaged AOD is shown from GACP (Figure 1c) [*Mishchenko et al.*, 2007], Collection 5.1 MODIS Level 3 Data Assimilation (DA) Quality (Figure 1e) [*Zhang et al.*, 2008], and AVHRR AERO100 (Figure 1g) [*Rao et al.*, 1989]. ESOA is apparent from three of these products (MODIS, MISR, and GACP), while the others (MODIS DA, SeaWiFS DeepBlue, and AVHRR) do not exhibit similar structure. It is plausible that ESOA reflects more stringent cloud screening applied to the MODIS DA, SeaWiFS DeepBlue, and AVHRR data sets, such as the “buddy check” system of investigating single data

points relative to surrounding ones as a supplemental and conservative spatial cloud-filtering step [e.g., *Zhang and Reid*, 2006; *Shi et al.*, 2011]. This hypothesis has yet to be evaluated, however.

[5] Ancillary measurements are available for comparing with these passive satellite composites. For an active-based satellite sensor perspective (Figure 1d), daytime AOD is shown for 1.0° by 1.0° three-year (2007–2009) averages from NASA Cloud-Aerosol Lidar with Orthogonal Polarization data sets (CALIOP; note that the methods used in constructing these averages are described later in the narrative, and we introduce them first here only as context) [*Winker et al.*, 2007; *Hunt et al.*, 2009]. CALIOP is a multiwavelength (532 and 1064 nm) polarization-sensitive elastic backscatter lidar flown within the NASA A-Train satellite constellation [*Stephens et al.*, 2002]. Similar to the MODIS DA, SeaWiFS DeepBlue, and AVHRR data sets described above, ESOA is not apparent in CALIOP retrievals. Further, 2.5° zonal AOD averages derived from hand-held Sun photometer measurements collected from ship-borne platforms and disseminated by the Maritime Aerosol Network (MAN) [*Smirnov et al.*, 2011] are shown from over the open waters of the Southern Hemisphere in Figure 1h for 2004–2009. Values are less than 0.08 across the Southern Ocean domain and thus lower than the apparently ESOA-biased data above as well.

[6] Aside from cloud contamination, there exist several plausible mechanisms for inducing ESOA, though they all involve some broad-scale effect on otherwise heterogeneous assumptions about surface brightness functions and boundary conditions underlying passive AOD retrievals. Some studies [e.g., *Lehahn et al.*, 2010; *Madry et al.*, 2011] suggest that

ESOA could be induced by high concentrations of sea salt aerosols due to strong near-surface ocean wind speeds associated with the “Roaring Forties” along this latitudinal band (e.g., white caps). One such study in particular, *Smirnov et al.* [2011], investigates the effect of wind speed on MAN AOD. They found a weak correlation between wind speed and AOD, with an increase in AOD on the order of 0.1 for a wind speed increase from 0 to 20 m/s. Others have proposed the potential for ESOA being associated with cloud halos (i.e., the “twilight zone” effect) [*Koren et al.*, 2007]. Underestimated/overestimated MODIS ocean surface albedo values and inaccurate aerosol models [e.g., *Shi et al.*, 2011], as well as cloud side-scattering effects [e.g., *Zhang and Reid*, 2006; *Wen et al.*, 2007; *Marshak et al.*, 2008], remain as other possible causes for ESOA.

[7] Clearly, discrepancies in optical property retrievals exist over the high-latitude Southern Oceans between many of the most prominent aerosol data sets used by the community. The domain is not of trivial size, and thus the potential impact on attempts to climatologically depict significant aerosol presence in regional and global climate models can be reflected by significant error within radiative and circulatory dynamic processes [e.g., *Koffi et al.*, 2012]. Whereas Figure 1 depicts well the disparity between available data sets from this region, two steps have yet to be pursued within the literature: first, that the bias quantitatively exists, and second, a proper assessment and decoupling of the physical mechanisms causing ESOA.

[8] In this paper, co-located MAN and MODIS AOD data sets over the Southern Oceans domain are investigated in order to determine whether or not a significant offset exists between the two. The benefits of active remote sensing are then leveraged through CALIOP, and the profiling of cloud hydrometeor and aerosol particle scattering, to study whether or not cloud presence, and subsequent/supplemental clearing of MODIS data sets, contributes significantly to ESOA (hence the use of MODIS data sets, collected in A-Train formation approximately 2 minutes ahead of CALIOP, versus those MODIS retrievals collected from the Terra platform). Therefore, the following research questions are addressed: Is ESOA the result of unscreened cloudiness? Do active profilers help screen the passive satellite data sets more thoroughly in order to suppress ESOA? If not fully to blame, to what magnitude is cloud contamination significant? What clouds (i.e., phase and vertical distribution) are passing through MODIS screening protocols and thus potentially impacting ESOA?

2. Ground-Based Context for Evaluating Passive Satellite ESOA Presence

[9] Ground-based AOD measurements from MAN (uncertainty of ± 0.02) [*Smirnov et al.*, 2011], combined with its parent Aerosol Robotic Network project (AERONET; uncertainty of ± 0.015) [*Holben et al.*, 1998], are considered benchmarks for aerosol particle optical properties observed worldwide [e.g., *Chin et al.*, 2002; *Yu et al.*, 2003]. MAN AOD data are collected through ship-borne operations where hand-held Microtops II Sun photometers are operated measuring AOD in five spectral channels ranging from 340 to 1020 nm [*Smirnov et al.*, 2011]. For consistency, as will be described with MODIS, AOD at 550 nm, derived from

the Level 2 MAN Spectral AOD product, is considered here. In the absence of a 550 nm channel, however, this value is calculated through interpolation from AOD measured at 500 and 675 nm using an Ångström relationship [e.g., *Shi et al.*, 2011].

[10] The first goal of this work is to consider MAN data relative to MODIS data sets in order to establish whether or not ESOA can be resolved and reconciled, and thus contrasted with the many passive data sets described above from which it is not found. Many studies have relied on AERONET data sets for validating passive satellite retrievals over the last decade [e.g., *Kaufman et al.*, 2005; *Shi et al.*, 2011; *Sayer et al.*, 2012]. However, over the Southern Oceans, the lack of land, and therefore the lack of possible AERONET coverage, leaves few remaining options for following such a well-established paradigm. MAN, however, despite having relatively few measurements in comparison to the wealth of data typically compiled from AERONET within comparatively sized domains, is practical for performing this task. Note that this is possible despite the majority of data points being collected in the summer hemispheric months, as opposed to the darker winter ones.

[11] For collocation and comparison, MAN data are required temporally to be within ± 30 min of a collocated MODIS retrieval and spatially within $\pm 0.3^\circ$ latitude/longitude [e.g., *Shi et al.*, 2011]. If these criteria are not met, no MAN comparison is performed. To increase the sample size, the northerly extent of the Southern Oceans domain is shifted slightly for this analysis to 40°S . MODIS Collection 5.1 Level 2 aerosol product (MYD04_L2) data sets are used, as reported at $10 \times 10 \text{ km}^2$ spatial resolution. The Effective_Optical_Depth_Best_Ocean (EODBO; 550 nm) and Cloud_Fraction_Ocean (CFO) parameters are considered (the latter being used since our domain is encapsulated almost solely by water at the surface). Note that the CFO represents the percentage of pixels excluded from retrieval processes, such as cloudy pixels and observations in glint regions [*Zhang et al.*, 2005]. The Quality_Assurance_Ocean (QAO) parameter is considered in order to constrain these two data sets to their highest potential quality. Retrievals flagged as either 1 (marginal), 2 (good), or 3 (very good) are thus included.

[12] Nearly 200 such MAN/MODIS co-locations are performed for the 2004–2011 period. These data are shown in Figure 2, beginning with a comparison of AOD reported by the two sensors in Figure 2a. Consistent with *Smirnov et al.* [2011], MODIS AOD are high relative to MAN observations by approximately 0.03. Similar results are also observed over coastal waters [e.g., *Adames et al.*, 2011]. Though these studies do not focus specifically on ESOA, their results are noted for context. Further, regardless of cloud fraction reported, a MODIS high bias exists. Higher biases are generally found for larger cloud fractions, indicating the likely impact of cloud contamination. MAN cloud screening is based on AERONET protocols, for which some incidence of sample bias due to misidentified cloudiness is possible. This is particularly evident with optically thin and spatially persistent cirrus cloud presence [*Chew et al.*, 2011], for which 0.03 compares well with estimates of effective optical depth thresholds of subvisual cirrus cloud occurrence [*Sassen and Cho*, 1992]. However, in spite of physical mechanisms for the moment, these findings are

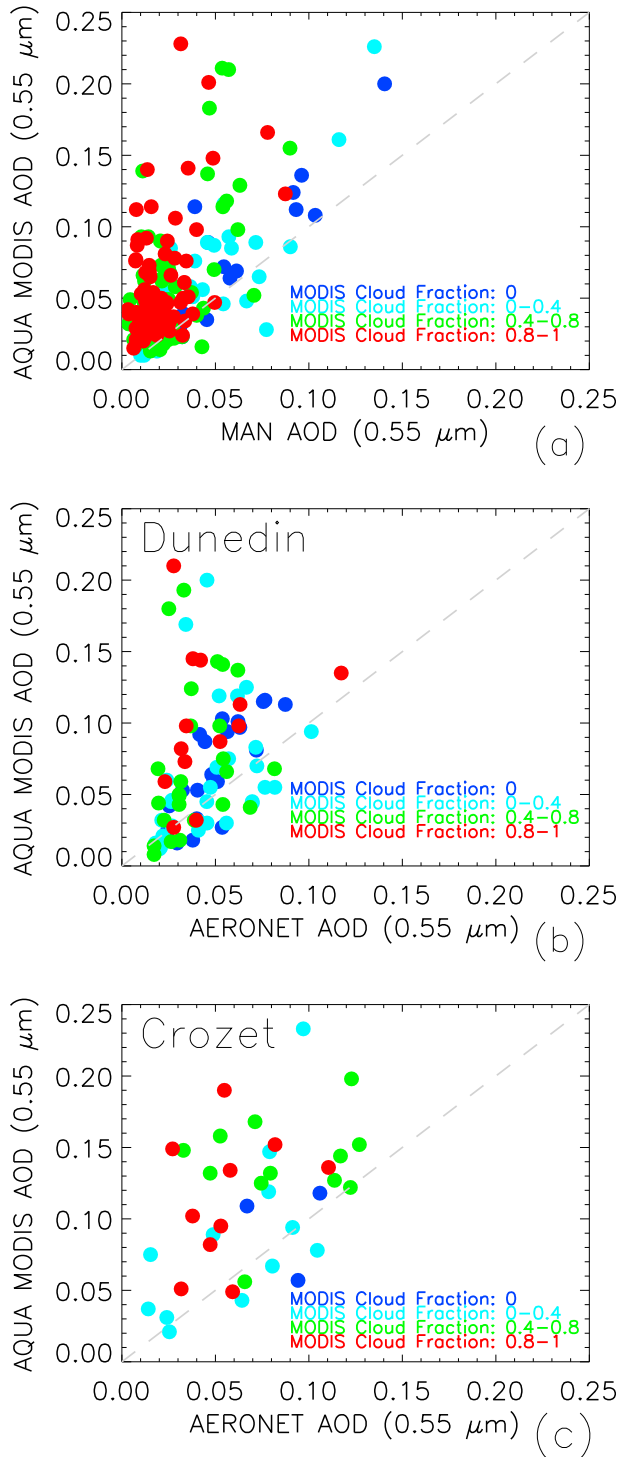


Figure 2. From 2004 to 2011, scatter plot of (a) MAN AOD for latitudes south of 40°S. From 2007 to 2009, scatter plot of (b) AERONET AOD at Dunedin, and (c) AERONET AOD at Crozet versus Aqua MODIS AOD.

broadly consistent with ESOA impacting MODIS retrievals over this domain.

[13] Two AERONET instruments have collected data in the Southern Oceans region during the 2007–2009 period: Dunedin (45.9°S, 170.5°E) and Crozet (46.4°S, 51.9°E). MODIS collocation here is the same as performed for

MAN, and AOD at 550 nm is calculated from AERONET Level 2.0 data using the same interpolation method of available/reported channels. A comparison of the 89 (Dunedin) and 37 (Crozet) available data points is shown in Figures 2b and 2c, respectively, for each site. Similar to the findings in the MAN comparison, MODIS AOD are uniformly larger than the AERONET estimates, again regardless of cloud fraction. While the highest MODIS AOD values generally correspond with larger cloud fractions, this pattern is not as pronounced as found versus MAN. Table 1 shows the mean values and data counts of MODIS, MAN, and AERONET 550 nm AOD for all points from each of the collocated samples described, as well as only those with a reported MODIS cloud fraction of 0.0. A large difference in mean MAN AOD (~0.027) exists between the “All” and “0.0 CFO” data sets. This is likely attributable to sample size, as data counts for the 0.0 CFO data set are more than 10 times fewer than the “All” data set. This discrepancy is consistent with *Jaegle et al.* [2011], as they showed seasonally averaged MODIS AOD from 2005 to 2008 was higher than AERONET at Dunedin and Crozet.

[14] Nearly 2400 MAN data points from 40°S to 70°S were used to construct Figure 1h and are included in this analysis. Thus, despite any sampling bias within MAN and AERONET data sets and relative to collocated MODIS samples, statistically, if ESOA actually existed over cloud-free skies or was the result exclusively of optically thin cirrus contamination, the signal should be observable from a multiyear analysis of MAN and/or AERONET data (e.g., Figures 1h and 2). However, we do not see such a signal for clear skies and can thus likely rule cirrus cloud contamination out as a significant factor.

3. Collocating CALIOP and Aqua MODIS AOD Data Sets to Study ESOA

[15] As suggested from the previous section, under cloud-free skies, the ESOA feature is not observed from ground-based observations using 8 years of MAN and 3 years of AERONET data. Therefore, questions arise, such as (1) is ESOA caused by cloud contamination? and (2) do passive sensors, like MODIS, observe ESOA under cloud-free skies? In this section, we attempt to address the above two questions by using aerosol and cloud products from CALIOP, as it exhibits much finer spatial and vertical resolutions (compared with MODIS) and thus has a better chance of detecting subpixel-sized clouds and cirrus. Both of these are sources of contamination for the MODIS aerosol products [e.g., *Zhang et al.*, 2005]. It is noted that differences in AOD between the two sensors are expected, as suggested by *Redemann et al.* [2012]. They showed that latitudinally averaged differences in AOD (MODIS-CALIOP) are usually less than 0.05, but may be as high as 0.1 in some latitude bands. *Kittaka et al.* [2011] and *Campbell et al.* [2012a, 2012b] show that these offsets vary when over land versus water, with MODIS data most frequently being high relative to CALIOP over the latter.

[16] For January 2007 to December 2009, MODIS data sets are co-located with two subsets of Version 3.01 CALIOP Level 2 5 km Aerosol Profile (L2_05kmAProf) product [*Winker et al.*, 2007; *Winker et al.*, 2012], one where cloud identification was available (i.e., successful cloud

Table 1. Mean Values and Data Counts of Aqua MODIS, MAN, Crozet, and Dunedin AOD for All Points in Each Data Set, As Well As Only Those With a MODIS Cloud Fraction of 0.0

Analysis	Number of Data Points		Mean AOD							
			MAN		Dunedin		Crozet		Aqua MODIS	
	All	0.0 CFO	All	0.0 CFO	All	0.0 CFO	All	0.0 CFO	All	0.0 CFO
MAN/Aqua MODIS	198	18	0.029	0.056	-	-	-	-	0.062	0.073
Dunedin/Aqua MODIS	89	21	-	-	0.046	0.051	-	-	0.072	0.069
Crozet/Aqua MODIS	37	3	-	-	-	-	0.070	0.089	0.111	0.095

algorithm retrievals) and another where aerosol particle profiling was available. CALIOP L2_05kmAProf data are reported at 5 km along-track resolution and used as the basis for co-location, described below. High-resolution layer type information (i.e., cloud versus aerosol) was obtained from the CALIOP Version 3.01 Level 2 Vertical Feature Mask (L2_VFM), which integrates the full range of CALIOP spatial averaging schemes applied for optimal layer detection and characterization [e.g., *Vaughan et al.*, 2009].

[17] MODIS and CALIOP co-location is based on spatial proximity. CALIOP and MODIS AOD observations are considered collocated when the center of a MODIS $10 \times 10 \text{ km}^2$ pixel is identified within 8 km of the temporal midpoint for a 5 km L2_05kmAProf profile. If this criterion is not met, no collocation is performed. This is similar to the collocation methodology of *Kittaka et al.* [2011], though their method is predicated on a 10 km separation between coincident points. *Campbell et al.* [2012a] and *Redemann et al.* [2012] also address the issue of collocating CALIOP and MODIS retrievals. Also, note that the collocation process utilized here considers only nadir viewing AOD measurements, given CALIOP’s nadir viewing track relative to the broader A-Train one. However, the MODIS retrieval accuracy may also be a function of viewing geometry such as viewing zenith angle [e.g., *Hyer et al.*, 2011; *Shi et al.*, 2011], for which any impact on ESOA cannot readily be addressed.

[18] For each collocation, an initial MODIS/CALIOP subset is generated for those data points where both valid MODIS EODBO and QAO values are reported in tandem with an equally valid L2_VFM record, and thus where 15 L2_VFM 0.333 km resolution profiles are found that correspond with the 5 km L2_05kmAProf profile. For this first subset, these data are considered irrespective of whether or not a valid aerosol profile was retrieved, thereby maximizing the amount of MODIS data available for study relative to CALIOP L2_VFM estimates of cloudiness. This subset is henceforth referred to as CALIOP_Cloud. A second, but not necessarily independent, subset is constructed for cases in which a valid L2_05kmAProf retrieval is available, and from which a CALIOP-iterated solution for column 532 nm AOD is subsequently derived [*Omar et al.*, 2009; *Young and Vaughan*, 2009]. Before deriving AOD, however, L2_05kmAProf extinction coefficient profiles are subject to supplemental QA screening. *Campbell et al.* [2012a] describe such a rubric for evaluating each profile bin, based on ancillary parameters reported in the L2_05kmAProf product. *Winker et al.* [2012] recently describe a new Level 3 aerosol profile product that features many of the same QA procedures. *Campbell et al.* [2012a] report that the differences between these two QA procedures are likely slight, however, and thus their method is

used to more efficiently pair L2_05kmAProf with the L2_VFM file. Also, following the data screening procedures of *Kittaka et al.* [2011], profiles composed of aerosol layers with integrated attenuated backscatter greater than 0.01 sr^{-1} are screened out. This subset is referred to as CALIOP_Aerosol. Note that points where an AOD equal to zero is solved after CALIOP QA screening are considered invalid and removed from the subset.

[19] For simplicity going forward, we discuss the respective 550 nm MODIS and 532 nm CALIOP AOD retrievals below without specifically referencing the wavelengths any further. It is further acknowledged that a slight difference when comparing AOD at these two wavelengths is to be expected and estimated at 3% considering an *Ångström* exponent relationship of 1.0 [e.g., *Kittaka et al.*, 2011]. Broad-scale analyses described below reflect a domain bounded from 60°S to 60°N, as a function of significant collocated sample size and context relative to the Southern Oceans. For brevity, however, these samples are referred to as “global.”

[20] For both subsets, cloud layers identified within an L2_05kmAProf average and reported in the L2_VFM product, are designated as either:

- [21] 1. Cirrus—cirrus clouds present only;
- [22] 2. Other—clouds present, but not distinguished as cirrus;
- [23] 3. Both—both Cirrus and Other are present;
- [24] 4. SF (Stratospheric Feature)—depicting the presence of polar stratospheric clouds or stratospheric aerosols;
- [25] 5. Clear—the column contains no cloud.

[26] Each layer classified as Other or Both is broken into seven possible feature subcategories, designated within L2_VFM. In the event that multiple sub-classifications occur within a single 5 km segment, the layer is assessed based on what feature is most prevalent relative to the number of bins classified in a single 0.333 km along-track profile (i.e., physical depth) multiplied by the number of profiles in which it is deemed present (i.e., temporal persistence). These subcategories are “low overcast, transparent” (LOT), “low overcast, opaque,” “transition stratocumulus” (TS), “low, broken cumulus” (LBC), “altocumulus (transparent)” (AT), “altostratus (opaque),” and “deep convective (opaque)” [*Liu et al.*, 2005]. Therefore, within the language applied by the L2_VFM product, Other represents a proxy for liquid water cloud presence. To limit the ambiguity in classifying a subcategory in the event that multiple types are present in equal depth and persistence, these few cases (less than 0.1%) are removed. Also, polar stratospheric clouds (PSCs) are not specifically identified and classified in the CALIOP data. Instead, CALIOP data only provide a very basic “stratospheric layer” classification that encompasses both PSCs (all types) and stratospheric aerosols. Also, such a

category represents a very small percentage of the data analyzed in this study (less than 1.0%). Therefore, we followed the same convention and labeled both stratospheric aerosols and clouds as Stratospheric Feature (SF). Lastly, low cloud flags (LBC, LOT, and TS) in the VFM data sets have exhibited questionable skill when evaluated by the CALIPSO Science Team, and changes to this product are pending future data releases. As a first-order estimate of cloud fraction, however, we apply the data here with this caveat implied in order to further cloud screen the data conservatively. As we will show, this does not significantly influence the final result.

[27] It is noted for the reader that, particularly with respect to cirrus clouds, the L2_VFM file includes clouds detected at horizontal averaging intervals in excess of 5 km L2_05kmAProf file (i.e., 20 and 80 km spatial resolutions). Thus, it is recognized that cloud identification from the VFM, and used for screening MODIS and CALIOP AOD subsets in the series of analyses described, can result in some measure of representativeness bias due to these extended averaging intervals [Yorks *et al.*, 2011]. However, as will become apparent, this serves to create the most conservative estimate of cloud presence possible from CALIOP, and thus relative to MODIS, which for the purposes of this study is believed an asset.

[28] For each subset (CALIOP_Cloud and CALIOP_Aerosol), three sets of analyses are performed, and described in the following section, using the collocated MODIS CFO and CALIOP L2_VFM data sets. The first represents MODIS AOD averages derived when $CFO \leq 1.0$, referred to as MODIS-100, which represents those EODBO AOD values where any cloud fraction (0.0–1.0) is allowed. Some past studies [e.g., Zhang *et al.*, 2005] have used a cloud fraction of 0.8 as an upper threshold, and thus a MODIS-80 (0.0–0.8 CFO) analysis is briefly shown later for context. However, this study utilizes cloud fractions of 0 and 1.0 as lower and upper limits in order to consider the maximum possible cloudiness. Second, an analysis is conducted when $CFO=0$, or when MODIS algorithms identify no clouds present within the bounds of the collocated $10 \times 10 \text{ km}^2$ pixel. This case is referred to as MODIS-0. Third, the latter sample is reexamined using the CALIOP L2_VFM product to eliminate any residual cloud-contaminated points identified with the lidar. This analysis is referred to as MODIS-CALIOP. Differences in mean AOD retrieved for each case, and in successive order of more thorough screening, are used to interpret the effects of cloudiness on MODIS AOD, identified both passively and actively, and consequently on ESOA. It is noted that a sampling bias exists between the MODIS and CALIOP footprints, and this is examined in greater detail later

in the text. However, this effect is less likely to be of concern for this study, as a significant number of data samples are used (see Table 2) to reduce such a bias.

[29] The two data sets, CALIOP_Cloud and CALIOP_Aerosol, have been delineated. The former considers all collocated MODIS points possible with information on potential cloud coincidence characterized from the lidar, and the latter allows for consideration of CALIOP AOD in order to establish context for comparison with MODIS AOD as a function of successive cloud-screening protocols. Total data points for each sample and the three corresponding analyses, along with their definitions and 3 year mean Southern Oceans AOD values, are given in Table 2.

[30] For this analysis, only annual statistics are shown. Some seasonality exists, however, between summer and winter composite results. The total number of data samples during Southern Hemisphere winter over the Southern Oceans domain is very limited, though, complicating the subsequent analysis. As such, we cannot significantly decouple the influence of cloud contamination on ESOA during this period in order to evaluate whether or not there are any relative decreases in MODIS AOD over the Southern Oceans that are seasonally based. Given that ESOA reflects a potential passive sensor artifact, and thus the ability to detect it is a function of number of total available data points from the relevant domain, and for which winter sample sizes are nearly three times lower than that of summer, we only acknowledge the scenario here with the goal of describing these results in greater seasonal detail in a future paper. This aspect of the study thus falls outside of the bounds of the narrative here.

4. Does Cloud Contamination Explain ESOA?

4.1. CALIOP_Cloud Subset Analysis

[31] Shown in Figure 3 are global distributions of 3 year (2007–2009) averaged MODIS AOD derived from the MODIS-100 analysis conducted for the CALIOP_Cloud subset. The granule-level collocated data are binned into 1.0° by 1.0° grid bins. Corresponding bin-resolved sample sizes are depicted for this analysis in Figure 3b. With no restriction on MODIS cloud fraction in these data, bands and specific regions of relatively high AOD are observed over both the high latitudes of the Northern Hemisphere and in the Southern Hemisphere as a result of ESOA. Despite polar-orbiting ground tracks, for which we would otherwise expect to have more samples in the higher latitudes from each hemisphere, these two regions exhibit the lowest numbers of observations per grid box. Instead, the highest observation densities are located in the latitude bands just

Table 2. For the CALIOP_Cloud and CALIOP_Aerosol Analyses, Each Subset Is Described (MODIS-100, MODIS-0, and MODIS-CALIOP), and Corresponding Data Point Samples and Mean AOD Are Reported

Analysis	Product Name	Criteria			Data Counts		Mean Southern Oceans AOD	
		CFO	CALIOP VFM	CALIOP AOD	Global Oceans	Southern Oceans	Aqua MODIS	CALIOP
CALIOP_Cloud	MODIS-100	0.0 – 1.0	Valid	-	9,835,710	779,337	0.158	0.086
	MODIS-0	0	Valid	-	1,978,417	166,313	0.107	0.067
	MODIS-CALIOP	0	Only clear; valid	-	1,656,337	141,416	0.101	0.065
CALIOP_Aerosol	MODIS-100	0.0–1.0	-	>0	8,007,967	584,851	0.143	0.075
	MODIS-0	0	-	>0	1,578,941	134,074	0.115	0.062
	MODIS-CALIOP	0	Only clear; valid	>0	1,331,613	115,022	0.110	0.061

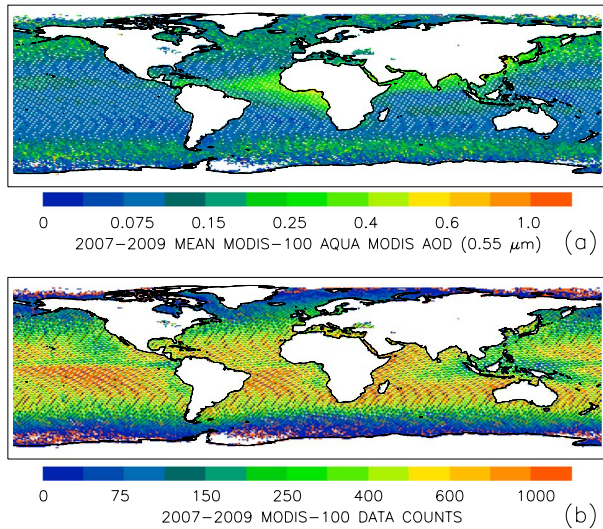


Figure 3. From 2007 to 2009, (a) MODIS-100 (CALIOP_Cloud subset analysis) Aqua MODIS Collection 5.1 global mean AOD from over-ocean “marginal,” “good,” and “very good” data sets and (b) their respective data counts, both displayed at $1.0^\circ \times 1.0^\circ$ resolution.

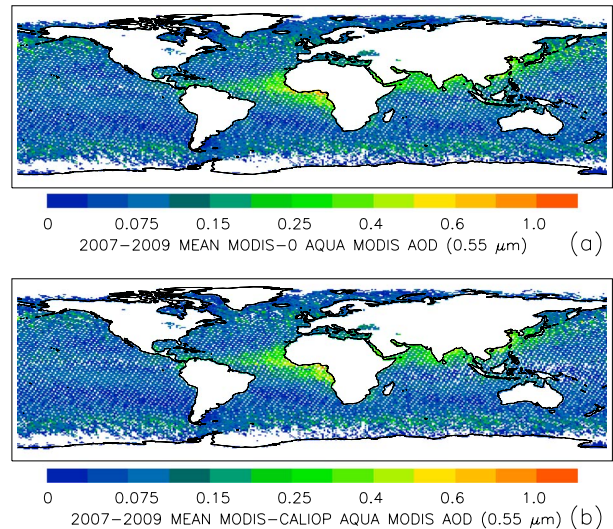


Figure 4. From 2007 to 2009, (a) MODIS-0 and (b) MODIS-CALIOP (CALIOP_Cloud subset analysis) Aqua MODIS Collection 5.1 global mean AOD from over-ocean “marginal,” “good,” and “very good” data sets, displayed at $1.0^\circ \times 1.0^\circ$ resolution.

south of the equator, as high latitudes experience winter seasons with much reduced data availability.

[32] Figure 4a features corresponding global AOD distributions for the MODIS-0 case, which includes the cloud-free restriction based on MODIS algorithms. Shown in Figure 4b is the corresponding MODIS-CALIOP analysis, with supplemental cloud screening applied to the MODIS-0 data using the CALIOP L2_VFM product. While high AOD values over the equatorial regions are still present in the MODIS-0 composite, reduced AOD are found over the Northern Hemisphere high latitudes and the Southern Oceans. However, despite active cloud detection conducted using the lidar for screening any residual cloudiness missed by MODIS, significant AOD differences are not readily apparent in the latter plot.

[33] These results are quantitatively depicted in Figure 5, which includes the corresponding zonal AOD averages at 1° meridional resolution between 60°S and 60°N as derived for each of the three analyses, in addition to the MODIS-80 analysis (for context). While the Southern Oceans region extends to 65°S , the domain of Figure 5 (along with Figures 6, 10, and 14) is plotted to 60°S due to a limited amount of available data further south. Significant change is observed between the MODIS-100 and MODIS-0 analyses, including an average AOD reduction of about 30–40% over the Southern Oceans that represents one of the highest such apparent residuals. Also, a slight decrease in AOD is observed between the MODIS-100 and MODIS-80 analyses. Some further reduction occurs between MODIS-0 and MODIS-CALIOP, though magnitudes are generally lower than 10%, and the Southern Oceans region experiences the lowest relative change observed globally. It is noteworthy that ESOA remains recognizable in the MODIS-CALIOP curve, when CALIOP and MODIS retrievals both do not detect clouds.

[34] The data are reassessed and re-depicted in Figure 6. In Figure 6a, the corresponding zonal mean of CALIOP

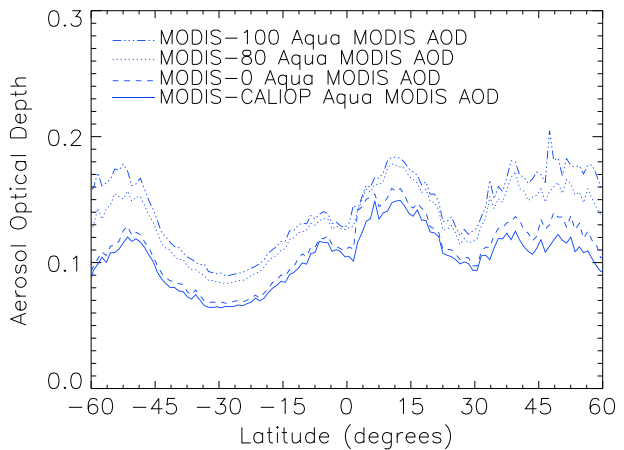


Figure 5. Three-year (2007–2009) global zonal mean of MODIS-100, MODIS-0, and MODIS-CALIOP (CALIOP_Cloud subset analysis) Aqua MODIS Collection 5.1 AOD data sets represented spatially in Figures 2 and 3.

L2_VFM layer classification percentage between 60°S and 60°N , for Clear, Cirrus, Other, Both, and SF is shown corresponding with the MODIS-100 (solid) and MODIS-0 (dashed) analyses. According to the L2_VFM product, zonal mean co-located MODIS-100 samples correspond with Clear at a rate roughly 40% of the time globally. Cirrus occurrence is found at maximum in the tropics, near 20%, and approaches 5–15% nearing the poles. Cases of Other vary greatly over the global domain, between 30% and 60%. They are highest over the Southern Oceans. Incidence rates for Both are lower than that of Cirrus, except again over the Southern Oceans. SF is mostly negligible. Notably, however, over the Southern Oceans domain, and unlike any other region, cases of Other are sampled more frequently than those of Clear.

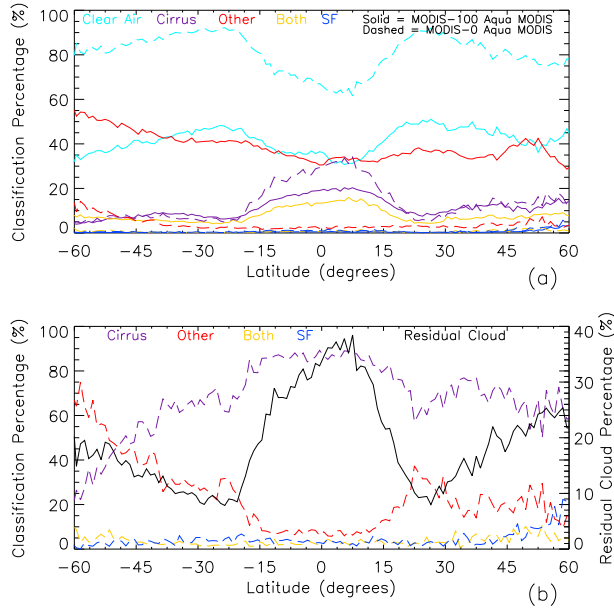


Figure 6. Three-year (2007–2009) global zonal mean of (a) CALIOP VFM classification percentages from MODIS-100 and MODIS-0 (CALIOP_Cloud subset analysis) and (b) percentage of residual cloud plotted with the relative percentages of particular cloud type of residual.

[35] When MODIS cloud screening is considered alone, cases of Other and Both drop significantly. The relative occurrence of Cirrus cases actually exceeds that found in the MODIS-100 sample in the tropics, in spite of the larger overall increase in Clear cases (>60%). MODIS cloud screening exhibits no apparent response to coincident cirrus cloud presence, as identified with CALIOP, as compared with liquid water-phase clouds [e.g., Ackerman et al., 2008]. In the MODIS-0 sample, Cirrus is identified more than Other north of 50°S. Over the Southern Oceans, clear air is the dominant scenario identified for this residual sample, with Other being the second most frequent.

[36] Since similar scrutiny of the MODIS-CALIOP analysis, as described from Figure 6a, would be completely cloud cleared, and thus all cases would be classified as Clear; instead, the relative residual between MODIS-0 and MODIS-CALIOP is displayed for each L2_VFM layer category in Figure 6b. Relative classification percentage and total percentage of residual cloudiness relative to the L2_VFM product identified in the MODIS-0 sample are shown for each zonal mean. Residual cloudiness is apparent within 10–40% of the MODIS-0 sample globally, highest in the tropics due mostly to cirrus clouds, and lowest at ~20°S and 25°N. Frequencies of residual cloudiness increase moving poleward (south and north, respectively) from the minima. As described above, over the Southern Hemisphere, cases of Other are most frequent, whereas in the north, cirrus clouds remain the greater contributor. Over the Southern Oceans, however, liquid water-phase clouds occur within the residual for between roughly 40% and 80% of the sample. This scenario is unique globally and plausibly reflects the dominance of ocean coverage along this band, and possibly marine-type cloudiness (investigated below).

[37] Sample sizes for Clear, Cirrus, Other, and Both are next investigated as a function of MODIS AOD. The MODIS-100 and MODIS-0 subsets are segregated into four corresponding MODIS AOD bins: <0.1, 0.1–0.2, 0.2–0.3, and >0.3. Figure 7a first details the classification percentages evaluated globally, for broader context. For MODIS AOD > 0.3, the MODIS-100 sample contains a larger presence of Other than Cirrus. The opposite is true, however, for the MODIS-0 analysis. Consistent with Figure 6a, through the use of MODIS cloud screening, cloud contamination from Both and Other cases is much reduced, yet the percentage of Cirrus remains mostly the same. This suggests that the cloud-screening process used by MODIS developers in their aerosol retrieval algorithms is less effective in identifying and eliminating cirrus relative to liquid water clouds [e.g., Gao et al., 2002].

[38] Focusing next on the Southern Oceans domain alone (Figure 7b), Other is the most prevalent non-Clear classification for both the MODIS-100 and MODIS-0 subsets for MODIS AOD greater than 0.3, but with a much reduced percentage in the MODIS-0 case. Considering the number of cases for the Other classification is larger than the Cirrus and Both classifications in the Southern Oceans region for the MODIS-100 and MODIS-0 subsets, we look at the cloud sub-classifications of the Other category (Figure 7c). For the MODIS-100 analysis, TS clouds exhibit the largest presence, while the MODIS-0 analysis reveals LBC is the primary cloud sub-classification. As such, TS and LBC likely cause the greatest cloud contamination of MODIS AOD retrievals over the Southern Oceans, though LBC is clearly the most important contributor to the MODIS-0 cloud residual. This point will become magnified below.

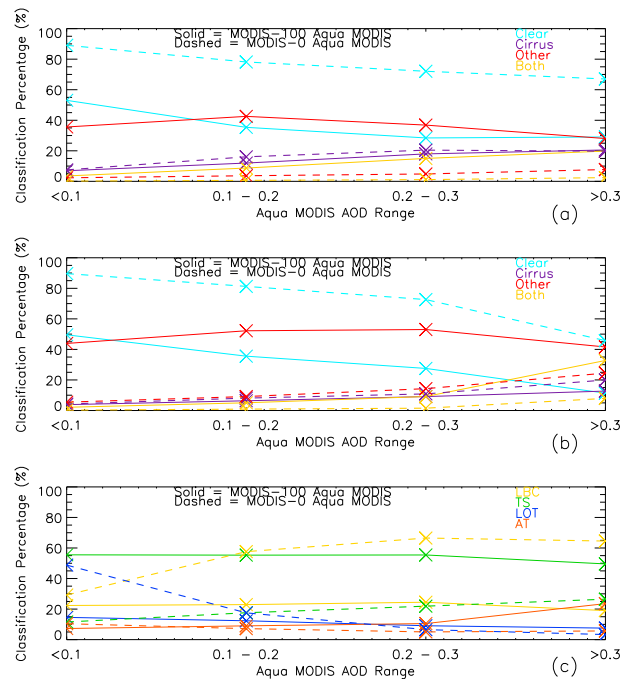


Figure 7. Three-year (2007–2009) CALIOP VFM classification percentages from MODIS-100 and MODIS-0 (CALIOP_Cloud subset analysis) for the (a) globe and (b) Southern Oceans region. (c) The relative sub-classification percentages of the “Other” classification shown in Figure 7b.

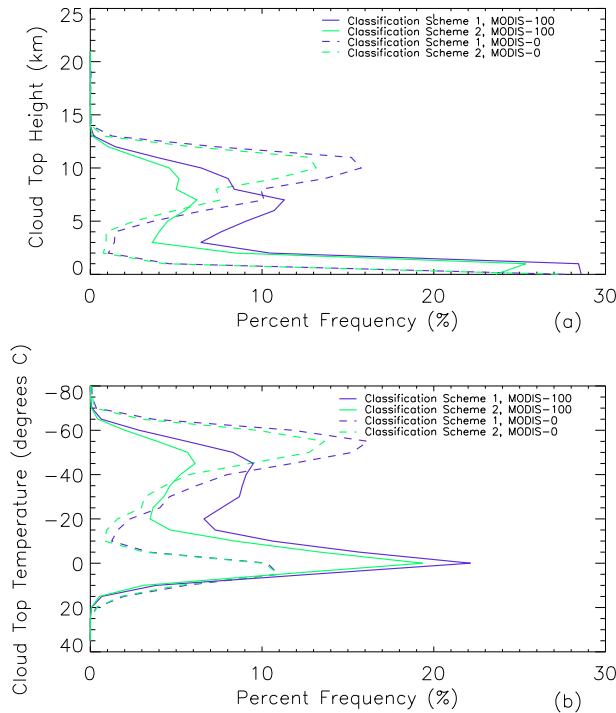


Figure 8. Vertical distribution of features classified by CALIOP VFM from the MODIS-100 and MODIS-0 CALIOP_Cloud subset analysis as a function of (a) height and (b) temperature using two classification schemes. See the text for the differences between the two schemes.

[39] In Figure 8, the vertical frequency distributions for cloud top height, in 1 km averaged bins (Figure 8a), and cloud top temperature, in 5°C bins (Figure 8b), are shown from the Southern Oceans domain for clouds identified with the L2_VFM in both the MODIS-100 and MODIS-0 samples. The latter case (MODIS-0) represents the residual cloud sample described above in Figure 6b, whereas the former (MODIS-100) is from the raw MODIS aerosol product. For each sample, two sets of frequencies are computed. For Classification Scheme 1, frequencies are derived for all clouds, thus accounting for cases where multiple cloud layers are present and nominally exceeding 100%. Classification Scheme 2 distinguishes multilayer cases by identifying only the one exhibiting the greatest temporal and spatial depth, and thus summing to 100% integrated frequency. Note that in Figure 8a, the vertical axis extends past 20 km above mean sea level (msl) from SF presence.

[40] The MODIS-100 distribution is seen to be bimodal, with the dominant mode centered at an altitude of ~1 km, corresponding to cloud top temperatures warmer than -10°C, as shown in Figure 8b. Colder/higher cloudiness is more broadly distributed, though frequencies do increase slightly with altitude. The distribution of the MODIS-0 residual is also bimodal, with distinct modes in cloud top height frequency apparent near 10 km above msl and again below 1 km msl. This corresponds with cloud top temperatures centered near -50°C and again above -10°C, respectively. The former represents cirrus cloud presence, since this mean cloud top temperature is well below -38°C, or the temperature for homogeneous freezing of liquid water that is believed

to be the predominant mechanism responsible for cirrus cloud presence [e.g., *Sassen and Campbell, 2001*]. The latter mode is representative of liquid water-phase cloudiness nearing the ocean surface and presumably embedded within the marine boundary layer.

[41] *Frey et al. [2008]* describe updates to the MODIS Collection 5 algorithm designed for better identifying stratocumulus clouds of limited horizontal extent, since cloud top radiances from these relatively warm clouds are difficult to differentiate from that of the background sea surface alone. That this lower/warmer mode represents the highest frequency for cloud presence identified in the Southern Oceans is potentially significant with respect to ESOA occurrence. However, it is interesting to note that there is no relatively significant mode for midlevel cloudiness with the MODIS-0 sample relative to MODIS-100 observed (e.g., altocumulus [*Gedzelman, 1988*], since these clouds can also be spatially fractured, physically thin, and seemingly a candidate for misidentification from passive sensors. This topic is reexamined below.

4.2. CALIOP_Aerosol Subset Analysis

[42] Next considered is the CALIOP_Aerosol analysis, which again is constructed for cases in which a valid L2_05kmAProf retrieval is available, and from which a CALIOP-iterated solution for column 532 nm AOD is derived. Figures 9a–9c depict global distributions of mean 1.0° × 1.0° CALIOP AOD derived for the MODIS-100, MODIS-0, and MODIS-CALIOP samples from CALIOP_Aerosol. Unlike Figure 3b, however, data point distributions are not shown. Sample sizes are again provided in Table 2, however. L2_05kmAProf QA screening removes roughly 20% of the data found from the CALIOP_Cloud sample, both globally and over the Southern Oceans. Qualitatively, very little change is apparent across each analysis from the corresponding MODIS composites. Consistent with Figure 1d, though, ESOA is not readily apparent in CALIOP-derived mean AOD at any stage of cloud screening (Figure 1d is Figure 9a). However, a different binning scheme, larger than 1.0° × 1.0°, may show enhanced AOD over the Southern Oceans. CALIOP algorithms do not detect any significant ESOA structure (e.g., the contrast of zonal-averaged AOD between 40°S to 60° S and 20°S to 40°S >0.03 at 550 nm).

[43] Shown in Figure 10a are zonal mean AOD averages between 60°S and 60°N at 1.0° meridional resolution for coincident MODIS and CALIOP data points from the CALIOP_Aerosol subset, respectively, for the MODIS-100, MODIS-0, and MODIS-CALIOP samples. Consistent with the CALIOP_Cloud subset, mean zonal AOD drops with each successive layer of MODIS and then CALIOP L2_VFM cloud screening. AOD peaks are observed from the MODIS data sets over the Southern Oceans and the tropical and high-latitude Northern Hemisphere. In contrast, CALIOP AOD are relatively consistent in the Southern Hemisphere, peak accordingly in the Northern Hemisphere tropics, and then conspicuously decline continuing along toward higher latitudes. Most importantly, however, it is clear from this analysis that supplemental CALIOP cloud screening does not suppress ESOA in the MODIS zonal mean (difference between the solid and dashed blue lines).

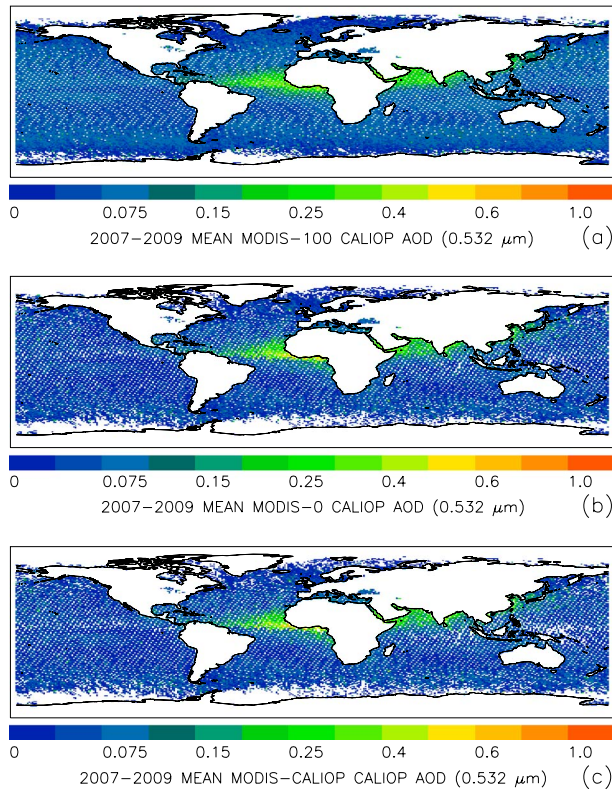


Figure 9. From 2007 to 2009, (a) MODIS-100, (b) MODIS-0, and (c) MODIS-CALIOP global mean CALIOP AOD for the CALIOP_Aerosol subset (see text) at $1.0^\circ \times 1.0^\circ$ resolution.

[44] Shown in Figure 10b are corresponding differences between MODIS and CALIOP mean zonal AOD for each sample analysis. The highest offsets between the passive and active instruments are found nearest the poles. Differences in the absolute magnitudes of the offsets between the samples are expected [Kittaka *et al.*, 2011; Campbell *et al.*, 2012a; Redemann *et al.*, 2012]. However, consider that much of the Northern Hemisphere includes land surfaces between 30° and 60°N , a region where maximum offsets are derived and pollution plumes exist. The Southern Oceans region thus stands out, as it lacks these significant and variable (i.e., not sea salt alone) surface particle sources zonally. Aerosol presence in a $10 \times 10 \text{ km}^2$ MODIS observation over this region can be presumed as fairly homogeneous, and thus both sensors should observe similar AOD distributions meridionally. Although similar issues also exist over the high-latitude Northern Hemisphere, the existence of transported aerosol plumes from major pollution sources such as Asia, Europe, and North America [e.g., Colarco *et al.*, 2004; Warneke *et al.*, 2006] complicates the issue, though for the purposes of this work, is believed to be a negligible effect.

[45] Figure 11 depicts the change in MODIS and CALIOP AOD between the MODIS-100 and MODIS-0 data sets (ΔAOD) as a function of a changing CALIOP cloud fraction (defined here as the relative occurrence frequency of cloudy profiles versus clear ones). Each data point represents a 1.0° zonal average of these two parameters for the Southern Oceans domain. The error bars represent the square root of the variance of the differences of mean AOD between the

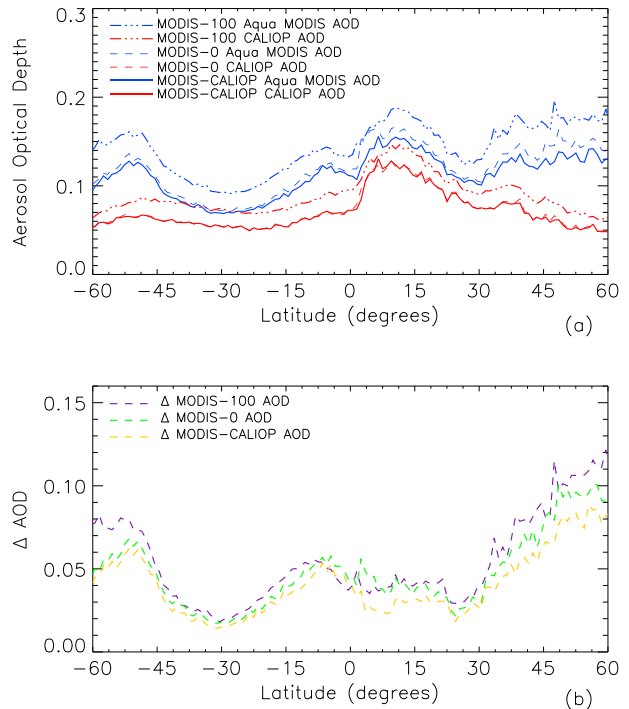


Figure 10. Three-year (2007–2009) global zonal mean of (a) Aqua MODIS AOD (in blue) and the respective CALIOP AOD (in red) for the CALIOP_Aerosol subset analysis, and (b) the AOD differences between Aqua MODIS and CALIOP for MODIS-100 (in purple), MODIS-0 (in green), and MODIS-CALIOP (in yellow).

two data sets. No relationship is found for the change in CALIOP cloud fraction and change in CALIOP AOD between the MODIS-100 and MODIS-0 data sets. The positive slope, however, apparent from the MODIS sample represents a correlation between cloud fraction and the passive-sensor AOD estimates. That is, the change in CALIOP cloud fraction introduces a change in zonal mean MODIS AOD but not CALIOP AOD, indicating likely cloud contamination over the ESOA region for MODIS.

[46] Relative differences in MODIS and CALIOP AOD are next interpreted with respect to L2_VFM scene and cloud classification. Beginning with the MODIS-100 analysis (Figure 12), Figure 12a depicts the frequency of occurrence for each layer classification category within the Southern Oceans domain, similar to Figure 6a, though now paired with respective mean MODIS and CALIOP-derived AOD. Consistent with Figure 6a, the most prevalent scenario identified with CALIOP is Other, or again liquid water clouds. Again, this scenario is unique to the Southern Oceans. Interestingly, MODIS AOD are higher for Cirrus cases than Other cases, and the differences between MODIS and CALIOP are relatively larger. This is even true when compared to the limited sample of SF cases.

[47] To distinguish what liquid water cloud types (i.e., phenomenology) are being identified from CALIOP within the MODIS-100/CALIOP_Aerosol subset, and thus for cases classified as Other and Both, respectively, Figures 12b and 12c include occurrence frequencies and corresponding mean MODIS and CALIOP AOD for the four most frequent cases of designated VFM cloud-type occurrence (the

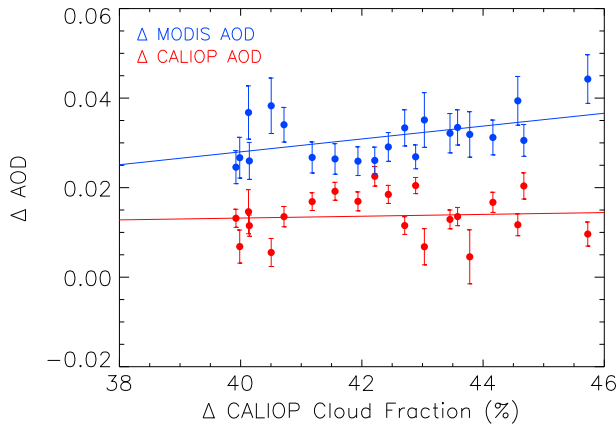


Figure 11. Scatter plot of the zonal mean change in CALIOP cloud fraction (as determined from the VFM) versus the zonal mean change in Aqua MODIS AOD from the MODIS-100 and MODIS-0 CALIOP_Aerosol subset analysis. Error bars represent the square root of the variance of the differences of mean AOD between the two data sets.

remaining cloud types are observed at very low frequencies and not shown). Relative AOD differences from each sensor for each classification are shown in Figure 12d. It is noted here that AOD differences may not solely be due to cloud contamination, but may also result from the algorithms themselves or detection limits. Since mean MODIS AOD are higher than CALIOP for cases of Both, the differences in this figure both relate to the corresponding value for Other subtracted from that of Both. TS clouds are most commonly identified when the scene is classified as Other, totaling over

50% of the sample. LBC is second, near 30%, and LOT is third at about 10%.

[48] The process is repeated in Figure 13, now for the MODIS-0 cloud residual. Here, however, and as seen above from Figure 6b, most of the cloudiness is suppressed. Cases of Other and Cirrus number about the same, while cases of Both and SF become very small. A change, though, in the type of clouds identified from the L2_VFM product occurs. For cases of Other, LBC cases now represent nearly 60% of the residual, though TS and LOT sum to about 40% combined. This change is primarily due to the reduction of TS cases from MODIS screening, as both LOT and LBC effectively double in relative frequency. AOD differences between Other and Both remain similar for TS and LBC, though they drop for LOT. The characteristics of the AT residual are mostly unchanged relative to the other scenarios.

[49] CALIOP algorithms distinguish between these three primary cloud types as a function of spatial persistence, quantified as a cloud fraction parameter solved from the relative number of clouds identified in 1 km segments with a top height below 3 km along an 80 km granule fetch [Liu et al., 2005]. Each type corresponds with a cloud top height pressure above 680 hPa and is transparent (i.e., the Earth’s surface was detected below the apparent cloud base). LOT cases are those where cloud fraction exceeds 0.98 (i.e., clouds detected in at least 79 of 80 one-kilometer profiles in a continuous 80 km segment). TS clouds are those where cloud fraction is less than 0.98 and exceeds 0.40 (approximate mean value ~0.7). LBC clouds are those where cloud fraction is less than 0.40 (approximate mean value ~0.2). Therefore, the drop in TS cases between MODIS-100 and MODIS-0 is consistent with MODIS algorithms exhibiting greater efficacy for distinguishing cloud presence

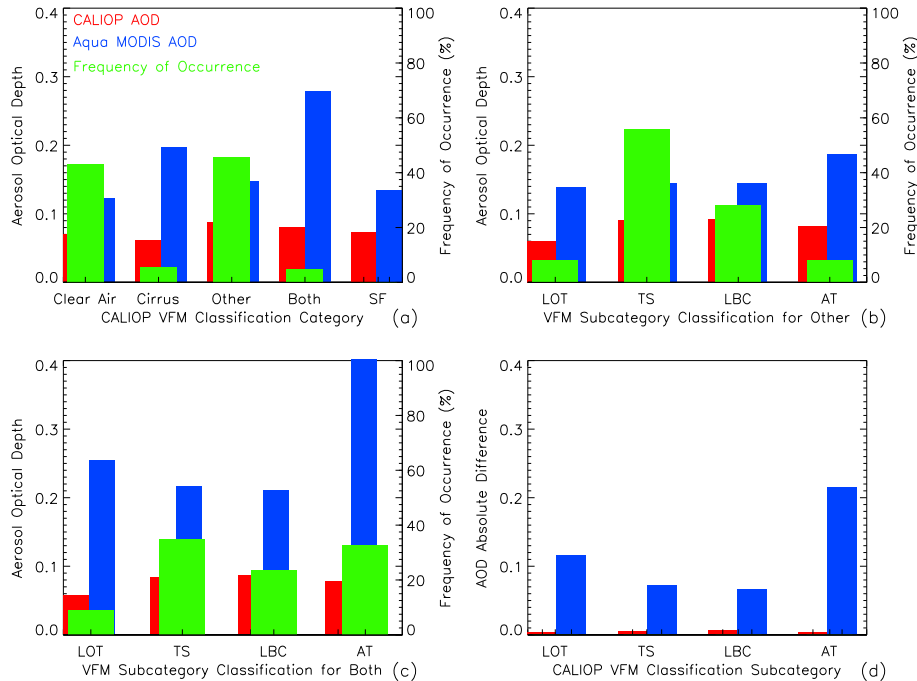


Figure 12. Three-year (2007–2009) average frequency of occurrence of (a) VFM classification categories, (b) “Other” subcategory classification, and (c) “Both” subcategory classification, and their respective Aqua MODIS and CALIOP AOD for the MODIS-100 CALIOP_Aerosol subset analysis. (d) The differences in Aqua MODIS and CALIOP AOD between the “Other” and “Both” subcategories.

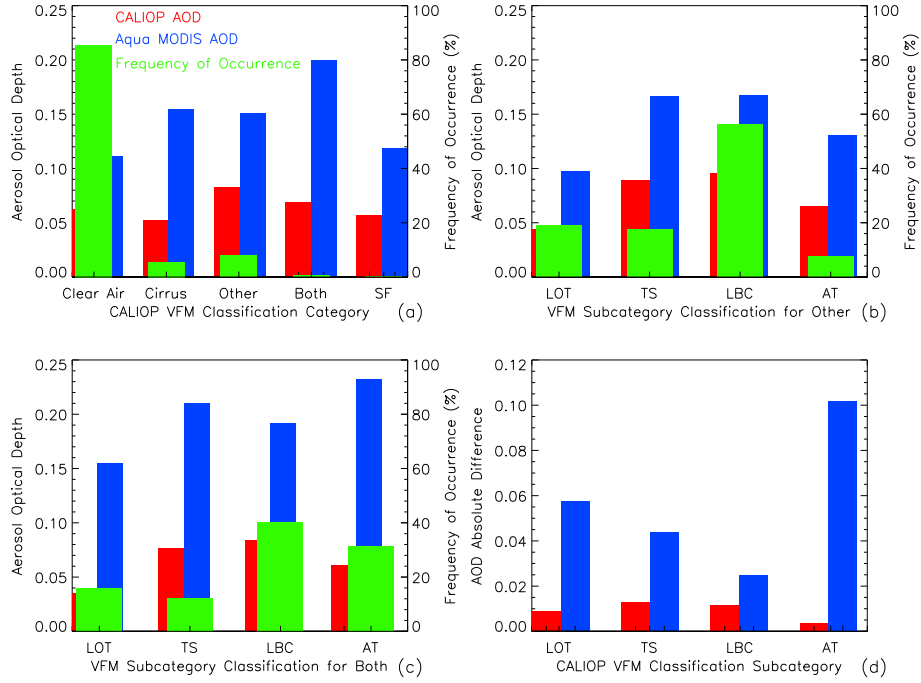


Figure 13. Three-year (2007–2009) average frequency of occurrence of (a) VFM classification categories, (b) “Other” subcategory classification, and (c) “Both” subcategory classification, and their respective Aqua MODIS and CALIOP AOD for the MODIS-0 CALIOP_Aerosol subset analysis. (d) The differences in Aqua MODIS and CALIOP AOD between the “Other” and “Both” subcategories.

for scenes with greater cloud fraction. For LOT, however, MODIS algorithm issues discriminating relatively warm clouds from the ocean surface below likely explain why those relative frequencies actually increase [e.g., Frey *et al.*, 2008].

[50] Since each of these three layer types may be transparent, this in fact may represent some undersampling in the CALIOP_Aerosol analysis from the requirement of a valid CALIOP aerosol and AOD retrieval corresponding with a collocated MODIS and CALIOP data point. For “low overcast, opaque” clouds, unless there is significant aerosol particle scattering above the cloud, and considering that full pulse attenuation occurs at some point within the cloud thus inhibiting sampling of an aerosol particle layer below it, these cases are being screened out in an unrepresentative manner. Comparing Figures 5 and 10a, in fact, the MODIS-CALIOP AOD analysis for CALIOP_Cloud is about 10% lower than that of CALIOP_Aerosol, which is likely attributable to this effect. This impact, however, is still low relative to the apparent ESOA offset from CALIOP_Aerosol (Figure 10a), as a whole.

[51] If CALIOP cloud fraction is considered representative of that for a collocated MODIS 10 km × 10 km composite data point, the finite sampling width of the laser footprint (70 m across the track, 330 m along the track at the surface) correlates with some statistical probability that the lidar will actually detect clouds within the bounds of the MODIS retrieval. The requirement that MODIS and CALIOP midpoints be within 8 km of one another does not guarantee that either a given CALIOP 5 km segment coincides with or falls entirely within the bounds of the collocated MODIS observation. However, most co-located data points have two CALIOP 5 km segments associated with the same MODIS 10 km × 10 km composite. One CALIOP 5 km segment,

given its surface footprint, translates to about 0.35 km² coverage compared with 100.0 km² area sample by MODIS. Thus, two 5 km CALIOP segments equal 0.7 km² coverage (rounded to a relative 1.0%). In this unique case where the profiled area is extremely small relative to MODIS, the probability for detection of a broken cloud scene converges to that of the cloud fraction itself. Otherwise, the solution would approach unity as the profiling swath approached that of the sampling area. Thus, for TS clouds and a mean cloud fraction of about 0.7, the probability of CALIOP detection [Kreyszig, 2006] is

$$1 - \frac{\binom{99!}{(70! \cdot 29!)}}{\binom{100!}{(70! \cdot 30!)}} = 0.7. \quad (1)$$

[52] For LBC clouds, this same calculation given a mean cloud fraction of about 0.2, results in a probability for detection of

$$1 - \frac{\binom{99!}{(20! \cdot 79!)}}{\binom{100!}{(20! \cdot 80!)}} = 0.2. \quad (2)$$

[53] Therefore, CALIOP cloud screening of the MODIS data is incomplete relative to the statistical probability that the lidar profile actually coincides with a cloud. TS and LBC are the only clouds reported in the L2_VFM with cloud fractions less than 1.0, and thus their relative incidence rates identified in the MODIS-0 residual are undersampled. To calculate the amount of this undersampling, we invert the solutions of equations (1) and (2), subtract 1.0, and multiply by 100%. This yields undersampling percentages of 42.8% for TS and 400% for LBC, and thus the MODIS-CALIOP

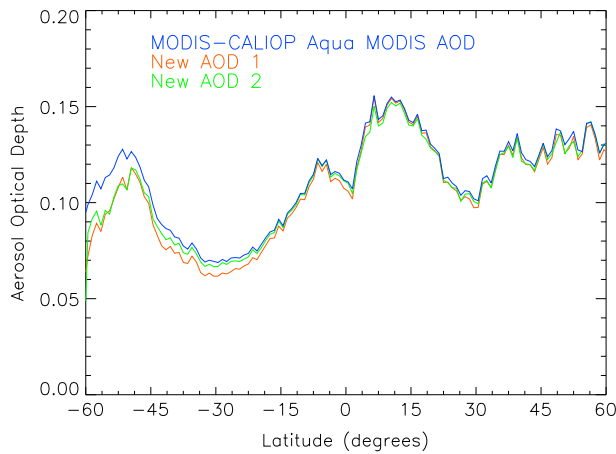


Figure 14. Three-year (2007–2009) global zonal mean of MODIS-CALIPOP Aqua MODIS AOD. Original is in dark blue and the corresponding renormalized AOD is in red (New AOD 1) and green (New AOD 2). New AOD 1 is computed using mean values of MODIS AOD for LBC and TS for the entire Southern Oceans region and are assumed to be constant throughout all latitudes. New AOD 2 is calculated using the zonal mean MODIS AOD for LBC and TS, and thus these vary with latitude.

sample actually remains cloud contaminated. Note that LOT clouds are not impacted by this, since cloud fraction is 1.0, corresponding with a 100% chance of detection and screening. Therefore, the MODIS-CALIPOP MODIS AOD profile shown in Figure 10a can be renormalized based on relative incidence rates and mean respective AOD at 1.0° meridional resolution to compensate for approximate TS and LBC undersampling.

[54] The renormalized MODIS-CALIPOP MODIS AOD global profile is shown in Figure 14, computed as

$$\text{New AOD} = \frac{(Z - HX - JY)}{K}, \quad (3)$$

where Z represents the zonal mean of MODIS-CALIPOP MODIS AOD. H and J are the approximated zonal percentages of undersampled LBC and TS points, respectively, computed using the number of LBC and TS points from the MODIS-0 analysis and the relative incidence rates shown above. X and Y are the average values of MODIS AOD for LBC and TS for the entire Southern Oceans region (reported in Figure 12b). As such, these values are presumed constant for each 1.0° zonal band due to small sample sizes in 1.0° meridional bands alone. K is the zonal percentage of uncontaminated points in the MODIS-CALIPOP MODIS sample, computed using

$$K = \frac{(F - (D + E))}{F} = 1 - H - J, \quad (4)$$

where F is the total number of points in the MODIS-CALIPOP sample (computed zonally), while D and E are the approximated zonal number of undersampled LBC and TS points from the MODIS-0 analysis, respectively, computed using the relative incidence rates described earlier. For a sensitivity analysis, a similar method is applied to find New AOD 2. This time, however, the values of X and Y are found using zonal averages of MODIS AOD for LBC and TS, and thus these values vary with latitude.

[55] Little difference is found in the new result globally, except over the Southern Oceans domain. However, even with these most stringent cloud-screening methods applied, a relative spike in zonal mean AOD is still observed over the Southern Oceans between MODIS (Figure 14) and CALIOP (Figure 10a). Though cloud contamination is clearly a factor in ESOA, it does not appear to be the sole contributor, and thus CALIOP screening alone cannot eliminate the ESOA feature in MODIS data sets.

5. Conclusions

[56] This paper investigates aerosol optical depth (AOD) retrievals from NASA Collection 5 Aqua Moderate Resolution Imaging Spectroradiometer (MODIS; $10 \times 10 \text{ km}^2$ mean value; 550 nm) co-located with Maritime Aerosol Network (MAN; 550 nm interpolated), Aerosol Robotic Network (AERONET; 550 nm interpolated), and Version 3.01 Cloud-Aerosol Lidar with Orthogonal Polarization (CALIOP; 5 km along-track average; 532 nm), data sets over the mid-to-high latitude Southern Oceans (defined as 45°S – 65°S) for an investigation of enhanced passive satellite values, referred to as the Enhanced Southern Oceans Anomaly (ESOA). The study of this phenomenon is important, as we find MODIS AOD biases much higher than the 0.01 benchmark set forth by the climate science community [e.g., *Chylek et al.*, 2003]. MODIS data are evaluated at multiple stages of cloud clearing, including MODIS algorithm cloud fraction estimates and comparison with CALIOP Level 2 Cloud Layer and Vertical Feature Mask data sets, in order to determine whether or not ESOA is the result of cloud contamination. Our study is summarized as follows:

[57] 1. First, we analyzed MAN and AERONET data against MODIS AOD retrievals to establish ground-based context for evaluating the presence of ESOA in some passive satellite retrievals over cloud free skies. MODIS AOD have a high bias of about 0.03 compared to MAN/AERONET. Statistically, if ESOA exists, its presence should be apparent from our multiyear analysis of ground-based data. However, our study shows that over cloud-free skies, ESOA does not exist in MAN and AERONET data, possibly due to two reasons: the ESOA phenomenon does not exist under cloud-free skies over the study area, or the current ground-based observations have a sampling bias and missed the scenarios for which ESOA could occur.

[58] 2. Next, we take advantage of the high spatial and vertical resolutions of CALIOP cloud detection capabilities to investigate whether or not this phenomenon is caused by cloud contamination. From this analysis, we conclude that cloud screening can significantly reduce ESOA (by about 30–40%), indicating that some of the ESOA signal can be attributed to unfiltered clouds. The largest contributors to cloud contamination are found to be stratocumulus and low broken cumulus clouds, even with the sampling bias of CALIOP.

[59] 3. A positive relationship is found between the change in MODIS AOD and that of CALIOP cloud fraction, which further suggests that cloud contamination exists in the retrieval process of some passive satellites

over the Southern Oceans region. However, even with the most stringent cloud screening (considering sampling bias), we are unable to completely remove ESOA from MODIS data sets. Further, it remains unclear where in MODIS retrievals and its technical proficiencies that differences from previous sensors exist, like SeaWiFS, so as to induce ESOA.

[60] 4. This bias may also be due to surface albedo assumptions and wind speed effects (e.g., white caps) [Lehahn *et al.*, 2010; Madry *et al.*, 2011]. The next data release for MODIS (Collection 6) may help alleviate the ESOA problem in this regard, as the new algorithms will include an improved multi-wind speed look up table [Kleidman *et al.*, 2012]. Other possible causes of ESOA are inaccurate MODIS aerosol models used in the retrieval process [e.g., Shi *et al.*, 2011], cloud-sidescattering effects [e.g., Zhang and Reid, 2006; Wen *et al.*, 2007; Marshak *et al.*, 2008], and floating ice in the Southern Oceans. A future field campaign may possibly help our understanding of ESOA from the aforementioned perspectives.

[61] 5. Through the use of CALIOP data, this study also investigates the cloud types that most commonly pass through MODIS cloud-screening algorithms. For the Southern Oceans region, liquid water phase clouds are the largest contributor to this residual cloudiness. This may be due to the large ocean coverage along this band, and possibly marine-type cloudiness. However, across all other areas of the globe, cirrus clouds are the most common type of residual cloud. This suggests the MODIS cloud-screening algorithms are more effective in identifying and eliminating liquid water clouds than cirrus clouds, except over the Southern Oceans.

[62] Since passive retrievals are based on indirect and multispectral techniques, identifying the physical mechanisms causing scenarios like ESOA is necessary for developing more robust algorithms. The skill of global visibility forecasting and mass transport modeling, and in particular those systems dependent on multivariate satellite data assimilation, is a function of the accuracy and representativeness of those inputs used for initialization [Zhang *et al.*, 2008]. Therefore, the ESOA scenario has implications for global aerosol observational and modeling systems, as evident in a recent study of mean AOD global distributions and annual trends [Zhang and Reid, 2010]. If not properly screened and accounted for, biases, such as ESOA, can potentially induce unnecessary error that negatively impacts any conclusions identified. Although this study shows that even active-based CALIOP screening does not remove this artifact alone, some improvement is still significant. Further, the distinguishing of cloud types most often missed by MODIS screening over open oceans has positive ramifications for improvements to these techniques globally.

[63] **Acknowledgments.** This research was funded through the support of the Office of Naval Research Codes 32 and 35. Author JRC acknowledges the support of NASA Interagency Agreement NNG12HG05I on behalf of the NASA Micropulse Lidar Network. Author YS acknowledges the support of the NASA Earth and Space Science Fellowship (NESSF) Program. CALIPSO data were obtained from the NASA Langley Research Center Atmospheric Science Data Center. MODIS data were obtained from NASA Goddard Space Flight Center. We acknowledge the AERONET and MAN programs, their contributing principal investigators and their staff for coordinating the sites and data used for this investigation.

Appendix

Acronym	Definition
AERONET	Aerosol Robotic Network
AOD	Aerosol Optical Depth
AT	AltoCumulus (transparent)
AVHRR	Advanced Very High Resolution Radiometer
CALIOP	Cloud-Aerosol Lidar with Orthogonal Polarization
CFO	Cloud Fraction Ocean
EODBO	Effective Optical Depth Best Ocean
ESOA	Enhanced Southern Oceans AOD
GACP	Global Aerosol Climatology Project
LBC	Low broken cumulus
LOT	Low overcast (transparent)
MAN	Maritime Aerosol Network
MISR	Multi-angle Imaging SpectroRadiometer
MODIS	Moderate Resolution Imaging SpectroRadiometer
MSL	Mean Sea Level
PSC	Polar stratospheric clouds
QA	Quality assurance
QAO	Quality Assurance Ocean
SeaWiFS	Sea-viewing Wide Field-Of View Sensor
SF	Stratospheric Feature
TS	Transition stratocumulus
VFM	Vertical Feature Mask

References

- Ackerman, S. A., R. E. Holz, R. Frey, E. W. Eloranta, B. C. Maddux, and M. McGill (2008), Cloud detection with MODIS. Part II: Validation, *J. Atmos. Oceanic Technol.*, *25*, 1073–1086.
- Adames, A. F., M. Reynolds, A. Smirnov, D. S. Covert, and T. P. Ackerman (2011), Comparison of Moderate Resolution Imaging Spectroradiometer ocean aerosol retrievals with ship-based Sun photometer measurements from the Around the Americas expedition, *J. Geophys. Res.*, *116*, D16303, doi:10.1029/2010JD015440.
- Campbell, J. R., et al. (2012a), Evaluating nighttime CALIOP 0.532 μm aerosol optical depth and extinction coefficient retrievals, *Atmos. Meas. Tech. Discuss.*, *5*, 2747–2794, doi:10.5194/amtd-5-2747-2012.
- Campbell, J. R., et al. (2012b), Characterizing the vertical profile of aerosol particle extinction and linear depolarization over Southeast Asia and the Maritime Continent: The 2007–2009 view from CALIOP, *Atmos. Res.*, doi:10.1016/j.atmosres.2012.05.007.
- Chew, B. N., J. R. Campbell, J. S. Reid, D. M. Giles, E. J. Welton, S. V. Salinas, and S. C. Liew (2011), Tropical cirrus cloud contamination in sun photometer data, *Atmos. Env.*, *45*, 6724–6731, doi:10.1016/j.atmosenv.2011.08.017.
- Chin M., P. Ginoux, S. Kinne, O. Torres, B. Holben, B. Duncan, R. Martin, J. Logan, A. Higurashi, and T. Nakajima (2002), Tropospheric aerosol optical thickness from the GOCART model and comparisons with satellite and sun photometer measurements, *J. Atmos. Sci.*, *59*, 461–483.
- Chylek, P., B. Henderson, and M. Mishchenko (2003), Aerosol radiative forcing and the accuracy of satellite aerosol optical depth retrieval, *J. Geophys. Res.*, *108*(D24), 4764, doi:10.1029/2003JD004044.
- Colarco, P. R., M. R. Schoeberl, B. G. Doddridge, L. T. Marufu, O. Torres, and E. J. Welton (2004), Transport of smoke from Canadian forest fires to the surface near Washington, D. C.: Injection height, entrainment, and optical properties, *J. Geophys. Res.*, *109*, D06203, doi:10.1029/2003JD004248.
- Diner, D. J., et al. (1998), Multi-angle Imaging SpectroRadiometer (MISR) instrument description and experiment overview, *IEEE Trans. Geosci. Remote Sens.*, *36*, 1072–1087.
- Frey, R. A., S. A. Ackerman, Y. Liu, K. I. Strabala, H. Zhang, J. R. Key, and X. Wang (2008), Cloud detection with MODIS. Part I: Improvements in the MODIS Cloud Mask for Collection 5, *J. Atmos. Oceanic Technol.*, *25*, 1057–1072.
- Gao, B. C., P. Yang, W. Han, R. R. Li, and W. J. Wiscombe (2002), An algorithm using visible and 1.38- μm channels to retrieve cirrus cloud reflectances from aircraft and satellite data, *IEEE Trans. Geosci. Remote Sens.*, *40*(8), 1659–1668.
- Gedzelman, S. D. (1988), In praise of altoCumulus, *Weatherwise*, *41*, 143–149.
- Holben B. N., et al. (1998), AERONET—A federated instrument network and data archive for aerosol characterization, *Rem. Sens. Environ.*, *66*, 1–16.
- Hunt, W. H., D. M. Winker, M. A. Vaughan, K. A. Powell, P. L. Luckner, and C. Weimer (2009), CALIPSO lidar description and performance assessment, *J. Atmos. Oceanic Technol.*, *26*, 1214–1228, doi:10.1175/2009JTECHA1223.1.
- Hyer, E. J., J. S. Reid, and J. Zhang (2011), An over-land aerosol optical depth data set for data assimilation by filtering, correction, and aggregation

- of MODIS Collection 5 optical depth retrievals, *Atmos. Meas. Tech.*, *4*, 379–408, doi:10.5194/amt-4-379-2011.
- Jaegle, L., P. K. Quinn, T. S. Bates, B. Alexander, and J.-T. Lin (2011), Global distribution of sea salt aerosols: New constraints from in situ and remote sensing observations, *Atmos. Chem. Phys.*, *11*, 3137–3157, doi:10.5194/acp-11-3137-2011, 2011.
- Kaufman, Y. J., et al. (2005), A critical examination of the residual cloud contamination and diurnal sampling effects on MODIS estimates of aerosol over ocean, *IEEE Trans. Geosci. Remote Sens.*, *43*, 2886–2897.
- Kittaka, C., D. M. Winker, M. A. Vaughan, A. Omar, and L. A. Remer (2011), Intercomparison of column aerosol optical depths from CALIPSO and MODIS-Aqua, *Atmos. Meas. Tech.*, *4*, 131–141, doi:10.5194/amt-4-131-2011.
- Kleidman, R. G., A. Smirnov, R. C. Levy, S. Mattoo, and D. Tanre (2012), Evaluation and wind speed dependence of MODIS aerosol retrievals over open ocean, *IEEE Trans. Geosci. Rem. Sens.*, *50*, 429–435, doi:10.1109/TGRS.2011.2162073.
- Koffi, B., et al. (2012), Application of the CALIOP layer product to evaluate the vertical distribution of aerosols estimated by global models: AeroCom phase I results, *J. Geophys. Res.*, *117*, D10201, doi:10.1029/2011JD016858.
- Koren, I., L. A. Remer, Y. J. Kaufman, Y. Rudich, and J. V. Martins (2007), On the twilight zone between clouds and aerosols, *Geophys. Res. Lett.*, *34*, L08805, doi:10.1029/2007GL029253.
- Kreyszig, E. (2006), *Advanced Engineering Mathematics*, Ninth edition, Wiley, 1248 pp., Hoboken, NJ.
- Lehahn, Y., I. Koren, E. Boss, Y. Ben-Ami, and O. Altaratz (2010), Estimating the maritime component of aerosol optical depth and its dependency on surface wind speed using satellite data, *Atmos. Chem. Phys.*, *10*, 6711–6720, doi:10.5194/acp-10-6711-2010, 2010.
- Liu, Z., A. H. Omar, Y. Hu, M. A. Vaughan, and D. M. Winker (2005), CALIOP algorithm theoretical basis document—Part 3: Scene classification algorithms. PC-SCI-202.03, NASA Langley Research Center, Hampton, VA 23681, 56 pp.
- Madry, W. L., O. B. Toon, and C. D. O'Dowd (2011), Modeled optical thickness of sea-salt aerosol, *J. Geophys. Res.*, *116*, D08211, doi:10.1029/2010JD014691.
- Marshak, A., G. Wen, J. A. Coakley Jr., L. A. Remer, N. G. Loeb, and R. F. Cahalan (2008), A simple model for the cloud adjacency effect and the apparent bluing of aerosols near clouds, *J. Geophys. Res.*, *113*, D14S17, doi:10.1029/2007JD009196.
- Mishchenko, M., et al. (2007), Long-term satellite record reveals likely recent aerosol trend, *Science*, *315*(5818), 1543–1543.
- Myhre, G., et al. (2004), Intercomparison of satellite retrieved aerosol optical depth over the ocean, *J. Atmos. Sci.*, *61*, 499–513.
- Myhre, G., et al. (2005), Intercomparison of satellite retrieved aerosol optical depth over ocean during the period September 1997 to December 2000, *Atmos. Chem. Phys.*, *5*, 1697–1719, doi:10.5194/acp-5-1697-2005.
- Omar, A. H., et al. (2009), The CALIPSO automated aerosol classification and lidar ratio selection algorithm, *J. Atmos. Oceanic Technol.*, *26*, 1994–2014.
- Rao, C. R. N., L. L. Stowe, and E. P. McClain (1989), Remote sensing of aerosols over the oceans using AVHRR data: Theory, practice and applications, *Int. J. Remote Sens.*, *10*, 743–749.
- Redemann, J., Vaughan, M. A., Zhang, Q., Shinozuka, Y., Russell, P. B., Livingston, J. M., Kacenelenbogen, M., and L. A. Remer (2012), The comparison of MODIS-Aqua (C5) and CALIOP (V2 & V3) aerosol optical depth, *Atmos. Chem. Phys.*, *12*, 3025–3043, doi:10.5194/acp-12-3025-2012.
- Remer, L. A., et al. (2005), The MODIS aerosol algorithm, products, and validation, *J. Atmos. Sci.*, *62*, 947–973.
- Sassen, K., and B. S. Cho (1992), Subvisual-thin cirrus lidar dataset for satellite verification and climatological research, *J. Appl. Meteor.*, *31*, 1275–1285.
- Sassen, K., and J. R. Campbell (2001), A remote sensing midlatitude cirrus cloud climatology: I. Macrophysical and synoptic properties, *J. Atmos. Sci.*, *58*, 481–496.
- Sayer, A. M., N. C. Hsu, C. Bettenhausen, Z. Ahmad, B. N. Holben, A. Smirnov, G. E. Thomas, and J. Zhang (2012), SeaWiFS Ocean Aerosol Retrieval (SOAR): Algorithm, validation, and comparison with other datasets, *J. Geophys. Res.*, *117*, D03206, doi:10.1029/2011JD016599.
- Shi, Y., J. Zhang, J. S. Reid, B. Holben, E. J. Hyer, and C. Curtis (2011), An analysis of the Collection 5 MODIS over-ocean aerosol optical depth product for its implication in aerosol assimilation, *Atmos. Chem. Phys.*, *11*, 557–565, doi:10.5194/acp-11-557-2011.
- Smirnov, A., et al. (2011), Maritime Aerosol Network as a component of AERONET—First results and comparison with global aerosol models and satellite retrievals, *Atmos. Meas. Tech.*, *4*, 583–597, doi:10.5194/amt-4-583-2011.
- Stephens, G. L., et al. (2002), The CloudSat mission and the A-Train: A new dimension of space-based observations of clouds and precipitation, *Bull. Amer. Meteorol. Soc.*, *83*, 1771–1790, doi:10.1175/BAMS-83-12-1771.
- Vaughan, M. A., K. A. Powell, R. E. Kuehn, S. A. Young, D. M. Winker, C. A. Hostetler, W. H. Hunt, Z. Liu, M. J. McGill, and B. J. Getzewich (2009), Fully automated detection of cloud and aerosol layers in the CALIPSO lidar measurements, *J. Atmos. Oceanic Technol.*, *26*, 2034–2050.
- Warneke, C., et al. (2006), Biomass burning and anthropogenic sources of CO over New England in the summer 2004, *J. Geophys. Res.*, *111*, D23S15, doi:10.1029/2005JD006878.
- Wen, G., A. Marshak, R. F. Cahalan, L. A. Remer, and R. G. Kleidman (2007), 3D Aerosol-cloud radiative interaction observed in collocated MODIS and ASTER images of cumulus cloud fields, *J. Geophys. Res.*, *112*, D13204, doi:10.1029/2006JD008267.
- Wielicki, B. A., R. D. Cess, M. D. King, D. A. Randall, and E. F. Harrison (1995), Mission to planet earth: Role of clouds and radiation in climate, *Bull. Amer. Meteor. Soc.*, *76*, 2125–2153.
- Winker, D. M., W. H. Hunt, and M. J. McGill (2007), Initial performance assessment of CALIOP, *Geophys. Res. Lett.*, *34*, L19803, doi:10.1029/2007GL030135.
- Winker, D. M., J. L. Tackett, B. J. Getzewich, Z. Liu, M. A. Vaughan, and R. R. Rogers (2012), The global 3-D distribution of tropospheric aerosols as characterized by CALIOP. ACPD, doi:10.5194/acpd-12-1-2012.
- Yorks, J., D. Hlavka, M. Vaughan, M. McGill, W. Hart, S. Rodier, and R. Kuehn (2011), Airborne validation of cirrus cloud properties derived from CALIPSO lidar measurements: Spatial properties, *J. Geophys. Res.*, *116*, D19207, doi:10.1029/2011JD015942.
- Young, S. A., and M. A. Vaughan (2009), The retrieval of profiles of particulate extinction from Cloud-Aerosol Lidar Infrared Pathfinder Satellite Observations (CALIPSO) data: Algorithm description, *J. Atmos. Oceanic Technol.*, *26*, 1105–1119.
- Yu H., R. Dickinson, M. Chin, Y. Kaufman, B. Holben, I. Geogdzhayev, and M. Mishchenko (2003), Annual cycle of global distributions of aerosol optical depth from integration of MODIS retrievals and GOCART model simulations, *J. Geophys. Res.*, *108*, 4128, doi:10.1029/2002JD002717.
- Zhang, J., and J. S. Reid (2006), MODIS aerosol product analysis for data assimilation: Assessment of over-ocean level 2 aerosol optical thickness retrievals, *J. Geophys. Res.*, *111*, D22207, doi:10.1029/2005JD006898.
- Zhang, J., and J. S. Reid (2009), An analysis of clear sky and contextual biases using an operational over ocean MODIS aerosol product, *Geophys. Res. Lett.*, *36*, L15824, doi:10.1029/2009GL038723.
- Zhang, J., J. S. Reid, and B. N. Holben (2005), An analysis of potential cloud artifacts in MODIS over ocean aerosol optical thickness products, *Geophys. Res. Lett.*, *32*, L15803, doi:10.1029/2005GL023254.
- Zhang, J., J. S. Reid, D. L. Westphal, N. L. Baker, and E. J. Hyer (2008), A system for operational aerosol optical depth data assimilation over global oceans, *J. Geophys. Res.*, *113*, D10208, doi:10.1029/2007JD009065.
- Zhang, J., and J. S. Reid (2010), A decadal regional and global trend analysis of the aerosol optical depth using a data-assimilation grade over-water MODIS and Level 2 MISR aerosol products, *Atmos. Chem. Phys.*, *10*, 10,949–10,963.